Check for updates

ChemElectroChem

Review
doi.org/10.1002/celc.202400365

Chemistry Europe
European Chemical Societies Publishing

www.chemelectrochem.org

Photoelectrochemical Hydrogen Production from Water Using Copper-based Chalcopyrite Thin Films

Shigeru Ikeda*[a] and Shogo Ishizuka[b]

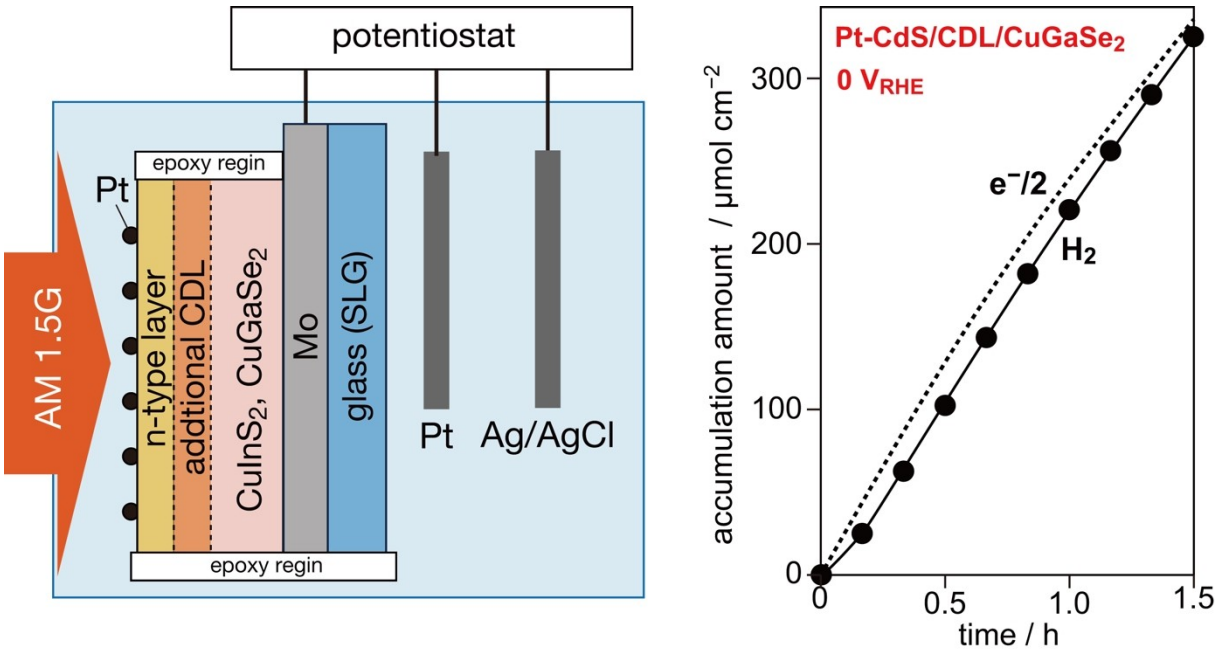

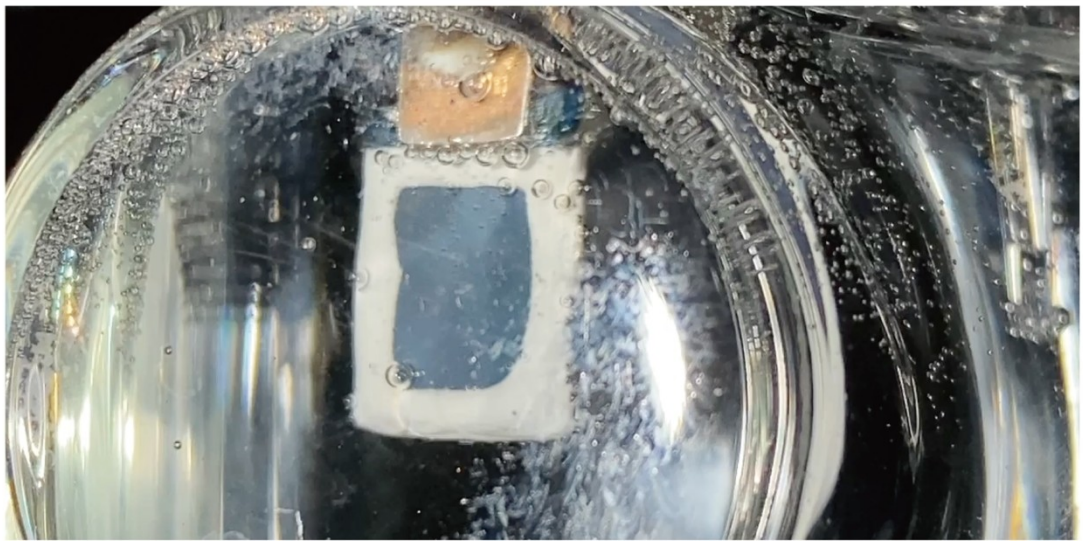

© 2024 The Authors. ChemElectroChem published by Wiley-VCH GmbH

21960216, 2024, 21, Downloaded from https://chemistry-europe.onlinelibrary.wiley.com/doi/10.1002/celc.202400365 by Chandigarh University, Wiley Online Library on [30/09/2026]. See the Terms and Conditions (https://onlinelibrary.wiley.com/terms-and-conditions) on Wiley Online Library for rules of use; OA articles are governed by the applicable Creative Commons License

Copper (Cu)-based chalcopyrite compounds are promising photoabsorber materials not only for solar cells but also for photoelectrochemical (PEC) systems for conversion of sunlight energy into chemical energy. PEC water splitting to generate hydrogen (H_2) is one of the most advanced technologies in a PEC system for the use of Cu-based chalcopyrite compounds. In this review, we firstly introduce crystallographic/energetic structures of Cu-based chalcopyrite compounds in view of their applications to PEC water splitting. Explanations for the operation of PEC water splitting using semiconductor materials are then overviewed. Based on these backgrounds, studies on PEC H_2 evolution over photocathodes based on $CuInS_2$ and $CuGaSe_2$ thin films that we have developed are reviewed in detail. For realizing efficient PEC H_2 evolution over these thin films, surface modifications with an n-type layer such as CdS and a catalytic site such as Pt deposit were found to be indispensable. Precise controls of p-n heterointerfaces formed by introducing an n-type layer should also be required to enhance PEC performance. Although PEC water splitting has not reached the required efficiency to be useful, effective combinations of appropriate surface and interface modifications should lead to further improvements of properties to be close to practical applications.

1. Introduction

Worldwide consumption of fossil fuels by human beings in 2022 was reported to be 494 EJ (exajoules).[1] This amount is equivalent to more than 80% of the total energy consumption worldwide. The reserve-to-production ratios (RPRs) of oil, natural gas and coal in 2020 were estimated to be about 54, 49 and 139 years, respectively. These facts indicate that oil and natural gas will be exhausted in the 21st century. The usage of fossil fuels has also caused serious environmental problems as well as global warming and climate change by the greenhouse effect due to a remarkable increase in the global emission of carbon dioxide (CO_2). Since more than 90% of the demand for fossil fuels is related to energy sources,[2] conversion to energy systems using renewable energy sources is a promising means for resolving the above-mentioned problems caused by huge consumption of fossil resources. Among the various kinds of renewable energy resources, utilization of solar energy is essential because of its abundancy and permanency. On average, the amount of solar energy reaching the earth's surface is estimated to 44 PW (4.4×10^{16} W), corresponding to 139×10^4 EJ per year.[3] This is a tremendous amount of energy compared to the total energy consumption by human society (604 EJ).

Significant fluctuation of sunlight intensity caused by changes in weather conditions, rotation of the earth, and season's transition lead to the requirement of storage technology. A solution for achieving low cost, long-term, and transportable storage is solar-to-fuel conversion, in which light energy in sunlight is converted into chemical energy in the form of gas or liquid fuels. Among the various kinds of fuels, hydrogen (H_2) is a promising medium because of its relatively high energy density per weight (120 MJ kg^{-1}) and the possibility of construction of a carbon-free substance circulation system. Moreover, H_2 can be utilized as a source of ammonia and methane, which are important commodity chemicals for modern society.

One possible method for achieving a realistic system using conventional technologies is water electrolysis in conjunction with electricity generated by solar cells. Actually, many examples based on commercially available electrolyzers and solar cells have been reported.[4] However, these devices often have critical problems of high capital expenditure and high operation costs due to the requirement of a complicated connection between the two devices and the use of costly materials such as noble metal electrocatalysts.[5]

The use of a powdered photocatalyst dispersed in a solution or embedded on a monolithic sheet is expected to become the most scalable and cost-effective device due to its simplicity. The first demonstration of direct photocatalytic overall water splitting was reported in the 1980's by using particulate metal oxides such as TiO_2 and $SrTiO_3$.[6] Since these oxide-based photocatalysts only absorb ultraviolet light, a photocatalyst that is visible light-responsive is required to achieve a meaningful solar-to-hydrogen conversion efficiency (STH) by using a photocatalytic system. Several photocatalysts have been reported, but the maximum STH of the photocatalysts is very low when compared to the solar conversion efficiency achieved by conventional solar cells. Based on the theoretical decomposition energy for water splitting reactions (1.23 eV), a semiconductor with a band gap energy (E_g) of ca. 1.4 eV, which is the optimum E_g for the spectrum of sunlight reaching the earth's surface, can provide a sufficient energy for water splitting. However, taking the requirement of overvoltage to induce electrocatalytic reactions into account, the required E_g would be larger than the optimal E_g. Photocatalytic systems require simultaneous reduction and oxidation of water on submicrometer-sized particles while suppressing carrier recombination and reverse reactions. Thus, the photocatalytic materials known so far have utilized wide-gap semiconductors that are not favorable for sunlight absorption.[7,8] A photocatalytic reaction system using a two-step photoexcitation process is often called a Z-scheme photocatalytic system. The system consists of two photocatalysts: one photocatalyst induces an H_2

[a] S. Ikeda
Department of Chemistry & Institute for Energy Conversion Materials, Konan University, Kobe, Hyogo 658-8501, Japan
E-mail: s-ikeda@konan-u.ac.jp

[b] S. Ishizuka
Global Zero Emission Research Center, National Institute of Advanced Industrial Science and Technology, Tsukuba, Ibaraki 305-8568, Japan
E-mail: shogo-ishizuka@aist.go.jp

© 2024 The Authors. ChemElectroChem published by Wiley-VCH GmbH. This is an open access article under the terms of the Creative Commons Attribution License, which permits use, distribution and reproduction in any medium, provided the original work is properly cited.

evolution reaction (HER) by water reduction and the other induces an O_2 evolution reaction (OER) by water oxidation on its surface.[9] By using two-step photoexcitation in two semiconductors, the voltage required for water splitting, including overvoltage, can be obtained, leading to possible usage of narrow-gap semiconductors that absorb light energy in the visible light region. As a recent example, a photocatalyst sheet in which $SrTiO_3$:La,Rh powder for HER and $BiVO_4$:Mo powder for OER were embedded showed a high STH value (1.2%).[9f] It should be noted that installation of an additional separation system such as a separation membrane is required because both single and Z-scheme photocatalytic systems generate a mixture of H_2 and O_2 gases.[10]

Another promising system using the two-step photoexcitation process is a photoelectrochemical (PEC) cell that is composed of two kinds of semiconductor electrodes: photocathode and photoanode for HER and OER, respectively.[11] Similar to the electrolyzer for overall water splitting, the HER and OER parts in the PEC cell are separated for each of the reactions. Therefore, the installation of a gas separation system that is required for the above-mentioned powder photocatalytic systems can be avoided in this system, though the connection of a unit for purification of evolved H_2 including de-oxidizer and drying sub-systems would be important for practical considerations.[12] An external bias voltage can be applied through a back contact layer to enhance water splitting. Moreover, appropriate surface modifications can be applied to each photoelectrode to improve its performances such as charge separation efficiency and stability. Among the various candidates of photocathodes and photoanodes, the authors have studied various Cu-based p-type chalcopyrite compound semiconductors, which are known as photoabsorption layer materials in thin-film solar cells, as effective photocathodes for HER.[13–15] In this paper, we thus focus on Cu-based chalcopyrite compounds for their applications as photocathodes for PEC H_2 evolution under sunlight irradiation. Following the description of several fundamental aspects of these compounds as well as the operating principle of PEC water splitting, the research history of photocathodes composed of Cu-based chalcopyrite compounds mainly developed in our laboratory is introduced in relation to several aspects and results discussed by other groups.

2. Features of Cu-Based Chalcopyrite Compounds as Photocathode Materials

Group I–III-VI_2 compound semiconductors are described as compounds derived from group II–VI semiconductors. Due to the ordered nature of atomic arrangements of groups I and III elements, however, they have a chalcopyrite structure similar to a two-layer structure rather than the sphalerite structure of group II–VI semiconductors (Figure 1).[16] On the other hand, it is also known that group II–IV–V2 compound semiconductors derived from group III–V semiconductors also have a chalcopyrite structure.[17] The discussion here will focus on I–III-VI_2 compounds (Cu-based chalcopyrite compounds) in which the group I element consists of Cu.

Copper indium selenide ($CuInSe_2$) is one of the I–III-VI_2 compound semiconductors composed of Cu (group I), In (group III), and Se (group VI) elements. This compound is a direct transition semiconductor with E_g of ca. 1.0 eV. The conduction band minimum (CBM) of the compound is mainly composed of the atomic orbital of In, whereas the valence band minimum (VBM) is derived from that of Se. Therefore, E_g of $CuInSe_2$ is altered by replacements of constituent elements, as shown in Table 1.[16b,18] For example, when the In site was replaced with lighter elements of Ga and Al, CBMs of the resulting compounds (i.e., $CuGaSe_2$ and $CuAlSe_2$) shifted upward relative to that of $CuInSe_2$, accompanied by a decrease in its lattice constants (Table 1). Moreover, E_g of the compound can be arbitrarily controlled by formation of mixed crystals. For example, a mixed crystal composed of $CuInSe_2$ and $CuGaSe_2$ (i.e., Cu(In,Ga)Se_2) with a Ga/(Ga + In) ratio of 0.3 has E_g of ca. 1.1 eV, the value of which is closer to the optimal value for sunlight absorption than that of $CuInSe_2$: the mixed crystal has been practically used as an absorber layer in photovoltaics.[19] Cu(In,Ga)Se_2-based photovoltaic solar cells and modules are now manufactured using multinary compounds consisting of a wide variety of elements such as (Ag,Cu)(In,Ga)$(S,Se)_2$; solar cells based on such compounds have demonstrated photovoltaic efficiencies as high as 23.35% for small area cells[20] and about 20% for modules.[21] The ability to promote photovoltaic properties through compositional control is a unique property not found in Si solar cells. It can also be compared with simpler binary



Shigeru Ikeda received his PhD from Tokyo Institute of Technology in March 1999. He had worked as an assistant professor in Hokkaido University until 2003 and was promoted to Associate Professor of Osaka University in 2003, having moved to Konan University as Professor in 2016. His major research interests are material development and device design for photocatalytic and PEC water splitting as well as that for solar cell based on compound semiconductors.



Shogo Ishizuka is currently a principal researcher of the National Institute of Advanced Industrial Science and Technology (AIST). He received his Ph.D. from the University of Tsukuba in 2003 and started working on Cu(In,Ga)Se_2 solar cells at AIST. From 2011, he worked for the National Renewable Energy Laboratory, as a visiting scientist for a year. He became a chief senior researcher in 2017, the team leader in 2018 and the group leader in 2020, and a prime senior researcher in 2022. His current research interests include chalcogenide materials for photovoltaic energy conversion devices such as solar cells and photoelectrochemical cells.

© 2024 The Authors. ChemElectroChem published by Wiley-VCH GmbH

21960216, 2024, 21, Downloaded from https://chemistry-europe.onlinelibrary.wiley.com/doi/10.1002/celc.202400365 by Chandigarh University, Wiley Online Library on [30/09/2026]. See the Terms and Conditions (https://onlinelibrary.wiley.com/terms-and-conditions) on Wiley Online Library for rules of use; OA articles are governed by the applicable Creative Commons License

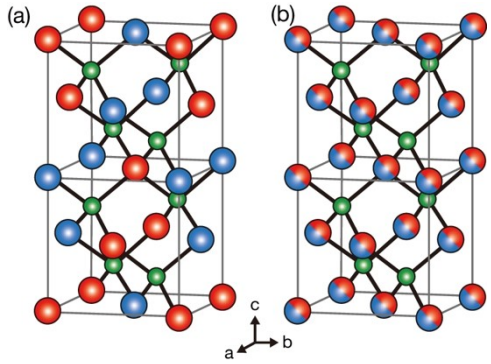

Figure 1. Conventional tetragonal cell of (a) chalcopyrite and (b) sphalerite. Red, bule, and green circles indicate group I, group III, and group IV atoms, respectively. In the (b) explicitly showing the Se tetrahedra surrounding the cations. groups I and III sphalerite structure, group I, group III atoms occupy their sites randomly.

Table 1. Bandgap energies (E_gs) and energy levels of the valence band maximum (VBM) and the conduction band minimum (CBM) from the vacuum level and crystallographic parameters of several Cu-based chalcopyrite compounds of several Cu-based chalcopyrite compounds.

Compound	E_g/ eV	VBM/ eV	CBM/ eV	*a*/nm	*c*/nm	*c*/*a*
$CuInSe_2$	0.99	−5.2	−4.1	0.5781	1.1642	2.01
$CuGaSe_2$	1.68	−5.2	−3.5	0.5612	1.1013	1.96
$CuAlSe_2$	2.72	−5.2	−2.5	0.562	1.121	2.00
$CuInS_2$	1.53	−5.4	−3.9	0.5522	1.1141	2.02
$CuGaS_2$	2.43	−5.5	−3.1	0.5351	1.0477	1.96
$CuAlS_2$	3.49	–[a]	–[a]	0.533	1.043	1.96

[a] Not reported.

compounds containing Cu, such as Cu_2O and Cu_2S, but the solar cell properties reported so far do not quite match those of systems based on a Cu-based chalcopyrite compound. Cu-based chalcopyrite materials are also advantageous for realizing lightweight and flexible thin-film devices, as their optical absorption coefficient is larger than that of Si and Cu_2O. Such features and facts are also significant for these materials in terms of their application in PEC systems, though several critical issues are also present (see below).

Various intrinsic defects should be included in $CuInSe_2$ and its derivatives because of their multinary natures. When relative strengths of chemical bonds in $CuInSe_2$ are considered, a Cu vacancy (V_{Cu}) is expected to form easily because the Cu–Se bond is a weak covalent bond, whereas the In–Se bond is a relatively strong ionic bond in $CuInSe_2$. Zhang et al. calculated formation energies of point defects in $CuInSe_2$ using first-principle calculations and found that Cu vacancies are the most likely acceptor-type defects responsible for the p-type electrical properties.[22]

As was discussed for solar cell devices based on the $Cu(In,Ga)Se_2$ thin-film absorber layer, there is no requirement to have a single-crystalline state for obtaining a high solar energy conversion efficiency. Although the origin of achievements of high efficiencies (i.e., low rate of carrier recombination) is still under discussion, several reports have suggested the occurrence of significant suppression of carrier recombination near grain boundaries (GBs) due to the formation of band bending (Figure 2).[23] In any case, a polycrystalline film of a chalcopyrite compound can be used; thereby possible uses of cost-effective methods for preparation of Cu-based chalcopyrite thin films are expected for future applications of them to various photodevices including devices for PEC water splitting.

3. Fundamentals of PEC Water Splitting Using Semiconductor Photoelectrodes

When a semiconductor electrode is immersed in an electrolyte, electron transfer occurs between the semiconductor and the electrolyte so that its Fermi level (E_F) is in equilibrium with the redox potential of the electrolyte. Since potential energies of the CBM and VBM at the solid-liquid interface are fixed, the electron transfer causes band bending to form a rectifying contact that is the same as that of a Schottky junction for a semiconductor-metal junction (Figure 3).[24] As a result, photogenerated electrons in the p-type semiconductor electrode accumulate at the solid-liquid interface (Figure 3a), whereas photogenerated holes in the n-type semiconductor electrode accumulate at the interface (Figure 3b).

If these accumulated carriers have sufficient potential to reduce or oxidize water, they can be used as a photocathode to reduce water to produce H_2 and a photoanode to oxidize water to produce O_2, respectively. The holes transferred to the electrode in the photocathode and the electrons transferred to the electrode in the photoanode are transferred to the counter electrode through a back contact and an external circuit, where they are used for oxidation and reduction, respectively. Because the potential energy of holes or electrons on the counter electrode corresponds to E_F of each photoelectrode in the photoexcited state, a semiconductor with a relatively high E_g must be used for such carriers to have the potential to reduce or oxidize water. Due to the circumstances, most semiconductors with E_gs in the visible light region do not have the potential

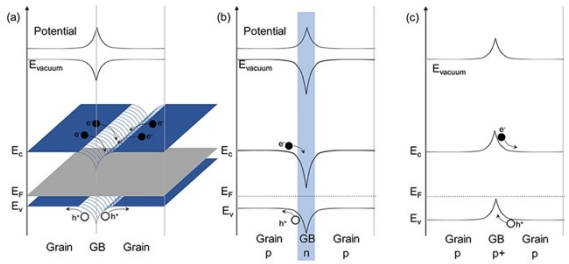

Figure 2. Schematic description of band bending near the grain boundary (GB) for (a) downward band bending at a GB, showing a three-dimensional (3D) depiction, (b) downward band bending including type inversion at a GB, and (c) upward band bending at a GB leading to accumulation of holes at the GB. Adapted with permission from Ref. [23e]. © 2018 American Chemical Society.

© 2024 The Authors. ChemElectroChem published by Wiley-VCH GmbH

21960216, 2024, 21, Downloaded from https://chemistry-europe.onlinelibrary.wiley.com/doi/10.1002/celc.202400365 by Chandigarh University, Wiley Online Library on [30/09/2026]. See the Terms and Conditions (https://onlinelibrary.wiley.com/terms-and-conditions) on Wiley Online Library for rules of use; OA articles are governed by the applicable Creative Commons License

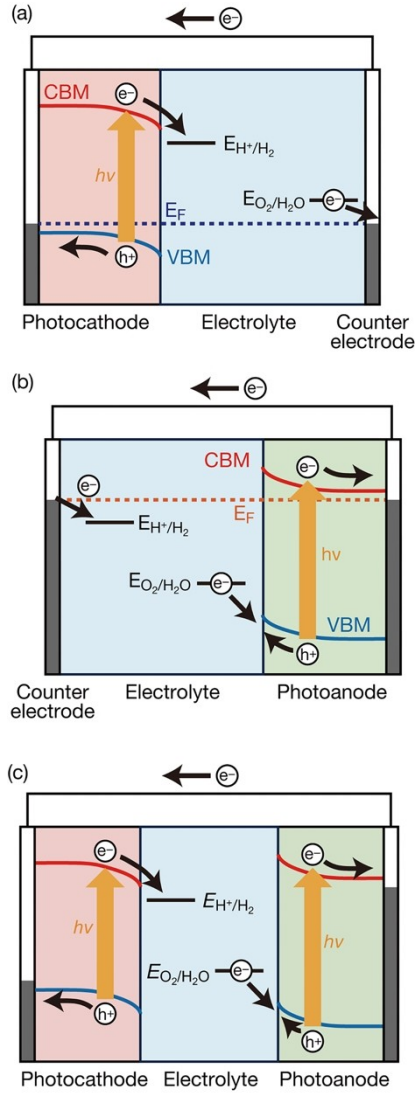

Figure 3. Energy diagrams of PEC water splitting using (a) a photoanode, (b) a photocathode, and (c) a photoanode and a photocathode in a tandem configuration. Symbols and abbreviations are noted in the main text.

to carry out overall water splitting at a single photoelectrode; the Cu-based p-type chalcopyrite compounds discussed here are no exception. In such cases, if a photocathode and photoanode are connected in series (tandem) and carriers with sufficient potential for water splitting reaction are generated by two-step photoexcitation, water splitting can proceed without external bias (Figure 3c). Although the tandem configuration requires two photons to obtain one electron (or hole) for use in the reaction, several semiconductor compounds that are responsive to visible light, which makes up most of the sunlight, can be used. According to calculations of STHs for PEC water splitting systems,[25] the maximum STH using a single photoelectrode is only about 13%, whereas in a tandem configuration, the value is expected to exceed 21%, which is equivalent to the efficiency of the current single-junction solar cells.

The simplest configuration for water splitting using a photoelectrode is a two-electrode system consisting of a photoelectrode and a counter electrode or a photocathode and a photoanode in a tandem configuration. In this system, E_Fs of both electrodes should ideally be the same as the equilibrium potential of the redox reaction occurring at the counter electrode. In actual operation, however, E_Fs do not match the equilibrium potential of the reaction at the counter electrode due to the overvoltage of the electrode reaction that depends on current density. When we focus on one electrode (called the "working electrode"), it is necessary to measure the current at the exact potential (current-voltage characteristic) to evaluate its intrinsic properties, which is not possible in a simple two-electrode system in which the potential is dependent on the properties of the counter electrode. Therefore, a three-electrode system, in which the potential of the working electrode is controlled by a potentiostat with respect to a reference electrode such as a saturated Ag/AgCl electrode, is often used for analyses of PEC performances of a newly developed electrode. The potential of the working electrode (E_{ref}) measured against the reference electrode (e.g., saturated Ag/AgCl electrode) can be converted to the potential against the reversible hydrogen electrode (RHE) (E_{RHE}) based on the following equation.

$$E_{RHE} = E_{ref} + 0.199 + 0.059 \times pH. \quad (1)$$

The equilibrium potentials for HER ($E_{H+/H2}$) and OER ($E_{O2/H2O}$) are unchanged at 0 V and +1.23 V, respectively, on the E_{RHE} basis, even when water splitting is performed using electrolytes with different pH values, leading to easiness for comparison of PEC properties measured in electrolytes with various pH ranges.

STH in PEC water splitting is defined as the ratio (in percentage) of the energy of H_2 produced by water splitting to the energy of sunlight. Therefore, when 1.0 kW m^{-2} of air mass 1.5 global tilt (AM1.5 G) is used as incident solar energy in a unit area, the STH value can be given by the following equation.[26]

$$STH\ (\%) = \frac{R_{H_2} \times 237}{1.0 \times S} \times 100, \quad (2)$$

where S and R_{H_2} denote the area of the photoelectrode in square meters (m^2) and the hydrogen production rate (R_{H2}) in a unit of mol s^{-1}, respectively. It should be noted that R_{H2} in this equation is regarded as the actual rate of H_2 production obtained in a two-electrode system. Thus, the value obtained in a system includes all factors affecting induction of overall water splitting reaction such as overvoltage of electrode reactions. In this case, if half the number of electrons per second (e$^-$/2 mol s^{-1}) passing through the external circuit (the conductor between the two electrodes) is equal to that of R_{H2}, i.e., the Faradaic efficiency (η_F) is unity, STH can be determined by the observed current. Since the current value in the PEC system is relatively simple to measure compared to quantitative measurement of the amounts of H_2 and O_2 produced, STH can be conveniently estimated from the current measurement.

© 2024 The Authors. ChemElectroChem published by Wiley-VCH GmbH

21960216, 2024, 21, Downloaded from https://chemistry-europe.onlinelibrary.wiley.com/doi/10.1002/celc.202400365 by Chandigarh University, Wiley Online Library on [30/09/2026]. See the Terms and Conditions (https://onlinelibrary.wiley.com/terms-and-conditions) on Wiley Online Library for rules of use; OA articles are governed by the applicable Creative Commons License

As mentioned above, the current-potential characteristic measured with a three-electrode configuration cannot directly determine STH from the current-potential curve because of feedback (by a potentiostat) to ignore the reaction (overvoltage) of the counter electrode. However, if the photoelectrode used as the working electrode generates H_2 or O_2 under sunlight (AM1.5 G) irradiation at a given potential at which water splitting does not proceed in the dark, a hypothetical half-cell STH (HC-STH) can be determined by the deviation from the equilibrium potential ($E_{H+/H2}$ or $E_{O2/H2O}$) and the photocurrent.[11c] If the operating potential during H_2 generation over a photocathode is fixed at a certain potential (E_{RHE}), the deviation from the equilibrium potential is written as E_{RHE}-$E_{H+/H2}$, corresponding to E_{RHE}. Moreover, when the current at the potential is I A over the photocathode having an area of S m^2, HC-STH is defined as follows.

$$\mathrm{HC-STH} = \frac{E_{\mathrm{RHE}} \times I \times \eta_{\mathrm{F}}}{1.0 \times 10^3 \times S} \times 100. \quad (3)$$

Again, HC-STH can be determined from current measurements when η_F is unity.

4. PEC Characterizations of a $CuInS_2$ Thin Film Deposited on a Molybdenum-Coated Glass Substrate

Investigation of PEC properties is useful for discussing the optoelectric properties of Cu-based chalcopyrite compounds as well as their energy levels of the CBM and VBM with respect to redox potentials of water oxidation and reduction. In order for these to be measured, a redox species capable of collecting photogenerated minority carriers is added to the solution. For p-type compound semiconductors, an electrolyte containing trivalent europium cation (Eu^{3+}) is commonly used because of the suitable potential of the Eu^{3+}/Eu^{2+} redox couple (−0.577 V vs. Ag/AgCl) to work as an efficient electron scavenger.[27] As the first trial of possible applications of Cu-based chalcopyrite compounds for PEC water splitting, we studied PEC properties of a polycrystalline $CuInS_2$ film in a solution containing Eu^{3+} with pH adjusted to 4 by using a conventional three-electrode setup (see above).[14a] The $CuInS_2$ film used was prepared on a molybdenum-coated glass substrate (Mo/glass) for a back contact from electrochemically stacked layers of metallic Cu and In followed by sulfurization in an H_2S flow.[28] The composition ratio of Cu and In (Cu/In) in the metallic precursor was fixed at a Cu-rich composition (Cu/In = ca. 1.3–1.4) compared to the stoichiometric ratio of the final $CuInS_2$ film. It is known that a high Cu/In ratio is desirable for obtaining a $CuInS_2$ film with high crystallinity and large grain sizes, due to the crucial role of the Cu_xS impurity phase(s) for accelerating the growth of $CuInS_2$ crystallites during the sulfurization process.[29] A slightly bluish gray color of the resulting film suggests surface coverage of Cu_xS components. Immersion of the thus-obtained film into a KCN solution (10%) induced selective dissolution of the binary Cu compound, as evidenced by disappearance of the bluish color of the film, whereas no structural alteration of the $CuInS_2$ part occurred with this treatment according to the results of X-ray diffraction of the film.

A linear sweep voltammogram of the thus-obtained $CuInS_2$ thin film deposited on Mo/glass at potentials from −0.55 to 0 (vs. Ag/AgCl) under chopped illumination from a 300 W xenon lamp showed a cathodic photocurrent flow, indicating that the $CuInS_2$ film prepared in the present study behaved as a p-type semiconductor electrode (Figure 4).[14a] The photocurrent onset appeared at −0.05 V (vs Ag/AgCl). Assuming that the onset of the present p-type semiconductor occurred at potentials of ca. 0.2 V more negative than the flat band potential (E_{fb}), E_{fb} of $CuInS_2$ in the present electrolyte solution lies at ca. 0.15 V (vs Ag/AgCl).

The photocurrent spectrum was measured using the lock-in technique. For this measurement, irradiation of the $CuInS_2$-based photocathode was performed by chopping at 10 Hz of monochromatic light, and the number of incident photons (N_p/mol s^{-1}) was determined by using a power meter. Intensity of the spectrum at each wavelength, defined as external quantum efficiency (EQE), was determined by using the following equation:

$$\mathrm{EQE} = \frac{I}{N_{\mathrm{p}} \times 96500}. \quad (4)$$

A typical spectrum obtained at −0.5 V vs Ag/AgCl is shown in Figure 5a. The onset region of the spectrum was analyzed to determine E_g of the present $CuInS_2$ electrode. As has been reported previously,[30] EQE can be related to E_g by the following equation:

$$\mathrm{EQE} \times h\nu = A\left(h\nu - E_{\mathrm{g}}\right)^{\mathrm{n}}, \quad (5)$$

where $h\nu$ is the incident photon energy and A is a proportionality constant, and n varies from 0.5 to 2.0 depending on the nature of the optical transition. Because the transition of the

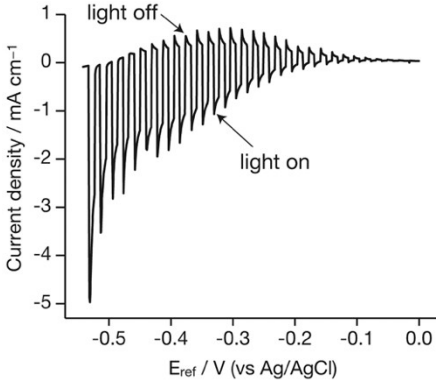

Figure 4. A linear sweep voltammogram of the $CuInS_2$ thin film deposited on Mo/glass in an aqueous $Eu(NO_3)_3$ solution (50 mM) under chopped illumination from a xenon lamp (300 W). Adapted with permission from Ref. [14a]. © 2011 Wiley-VCH.

© 2024 The Authors. ChemElectroChem published by Wiley-VCH GmbH

21960216, 2024, 21, Downloaded from https://chemistry-europe.onlinelibrary.wiley.com/doi/10.1002/celc.202400365 by Chandigarh University, Wiley Online Library on [30/09/2026]. See the Terms and Conditions (https://onlinelibrary.wiley.com/terms-and-conditions) on Wiley Online Library for rules of use; OA articles are governed by the applicable Creative Commons License

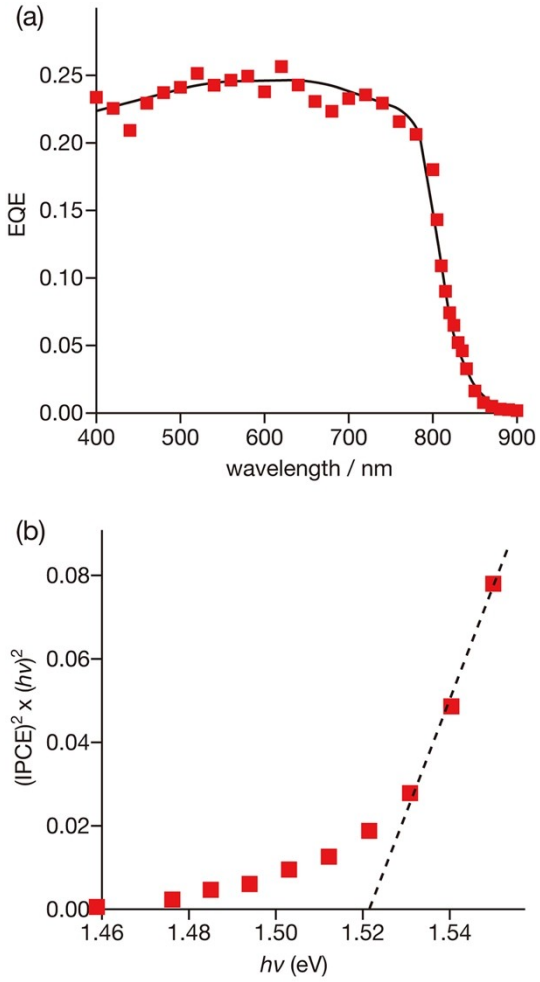

Figure 5. (a) External quantum efficiency (EQE) plots of the $CuInS_2$ film measured at 0.5 V vs Ag/AgCl in an aqueous $Eu(NO_3)_3$ solution (50 mM) under irradiation of monochromatic light with various wavelengths. (b) Plots of $(EQE)^2 \times (h\nu)^2$ vs $h\nu$ for the $CuInS_2$ thin film. An intercept line denotes the E_g value. Adapted with permission from Ref. [14a]. © 2011 Wiley-VCH.

$CuInS_2$ compound is known to be direct (see above), n of 0.5 is applied to them. Figure 5b shows the plot of $(EQE)^2 \times (h\nu)^2$ against $h\nu$ for the $CuInS_2$ electrode. Since a linear relation was obtained as predicted by Equation (5), E_g was determined from the intercept of the photon energy ($h\nu$) axis. The E_g value was determined to be ca. 1.52 eV, which is almost the same as the reported E_g value of 1.53 eV.[18a] Based on the above results, the CBM and VBM were estimated to lie at −1.3 V and 0.2 V (vs Ag/AgCl), respectively. In the pH region, the CBM is likely to be 0.9 V negative compared to the potential of $E_{H+/H2}$, indicating sufficient potential for water reduction. On the other hand, the fact that the VBM is more than 0.6 V higher than $E_{O2/H2O}$ rules out the possibility of overall water splitting on this electrode in a single-junction configuration.

5. Attempts for Efficient Water Reduction into H_2 Using Cu-Based Chalcopyrite Electrodes

PEC properties for HER over the $CuInS_2$-based photocathode were examined by using the above-mentioned three-electrode setup. Figure 6a shows a current-potential curve of the electrode in an Na_2SO_4 solution with pH adjusted to 4. The electrode composed of the bare $CuInS_2$ film deposited on Mo/glass showed little photoresponse, indicating low activity of the bare $CuInS_2$ surface for water reduction. In order to facilitate the reaction, nanoparticulate Pt was loaded on the surface of the $CuInS_2$ film by using a photodeposition method. As a result, appreciable increases in photocurrents were achieved by using the electrode (Pt-$CuInS_2$) owing to the effectiveness of loading Pt deposits as promoters for HER (Figure 6b). In order to improve the photoresponse of the Pt-$CuInS_2$ electrode, we attempted to deposit an additional n-type layer over the p-type $CuInS_2$ photocathode to facilitate charge separation efficiency through formation of a hetero-type p-n junction. Among various materials and methods, we chose a cadmium sulfide (CdS) thin layer with a thickness in a scale of several tens of nanometers deposited by the chemical bath deposition (CBD) method because the CdS-based heterojunction obtained by the CBD method has been studied in detail for its application in solar cells based of the $Cu(In,Ga)Se_2$ photoabsorber layer. Figure 6c shows typical current-potential curves of the film followed by loading of Pt deposits (i.e., Pt-CdS/$CuInS_2$). It is clear that insertion of the n-type layer significantly improved cathodic photocurrents.[14] Moreover, the modification led to

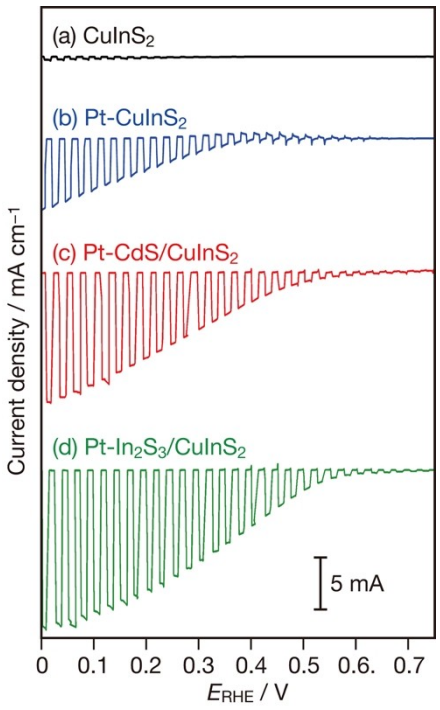

Figure 6. Current density-potential curves for (a) $CuInS_2$, (b) Pt-$CuInS_2$, (c) Pt-CdS/$CuInS_2$, and (d) Pt-In_2S_3/$CuInS_2$ electrodes. Electrolyte: 0.2 M NaH_2PO_4 aq. (pH 6). Light source: simulated sunlight (AM 1.5 G) (chopped illumination).

© 2024 The Authors. ChemElectroChem published by Wiley-VCH GmbH

21960216, 2024, 21, Downloaded from https://chemistry-europe.onlinelibrary.wiley.com/doi/10.1002/celc.202400365 by Chandigarh University, Wiley Online Library on [30/09/2026]. See the Terms and Conditions (https://onlinelibrary.wiley.com/terms-and-conditions) on Wiley Online Library for rules of use; OA articles are governed by the applicable Creative Commons License

appreciable positive shifts of onset potentials of more than 0.1 V (ca. 0.59 V vs RHE).

In the same period, Domen et al. also reported the effectiveness of the use of a CBD-derived CdS layer in a PEC H_2 evolution system by using a Cu(In,Ga)Se_2-based photocathode.[13a] Further studies on the effect of the CdS modification were also performed by the same group using a $CuGaSe_2$-based photocathode: semi-quantitative calculations of the built-in electric fields of electrolyte-$CuGaSe_2$ thin film interfaces without and with a CdS layer by using Poisson's equations suggested that the presence of CdS led to an increase in the depletion layer width at a certain potential, indicating an enhancement of carrier separation at the interface region of the $CuGaSe_2$ thin film (Figure 7).[13b]

As other examples of n-type layers, we have demonstrated the effectiveness of a CBD-deposited ZnS or In_2S_3 layer for the $CuInS_2$-based photocathode.[14b,c] For the case of In_2S_3, transmittance spectra of CdS and In_2S_3 layers deposited on a fluorine-doped tin oxide (FTO) glass substrate indicated appreciably higher transparency of the In_2S_3 layer than that of the CdS layer at this energy region. The better transparency of In_2S_3 should lead to efficient photoabsorption (i.e., carrier generation) at the bottom $CuInS_2$ layer in the electrode (Pt-In_2S_3/$CuInS_2$). This is one of the advantageous features for PEC water splitting, i.e., achievement of a relatively large photocurrent density and positive onset over the Pt-In_2S_3/$CuInS_2$ electrode compared to that of the Pt-CdS/$CuInS_2$ electrode (Figure 6 d).[14b]

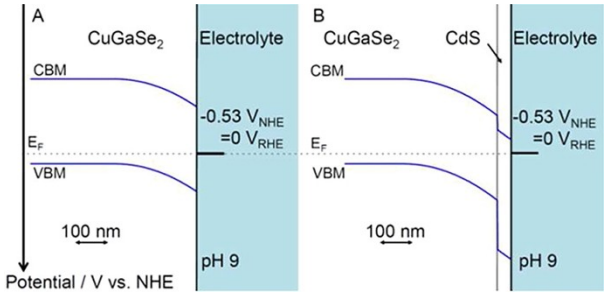

Figure 7. Calculated band alignment at the solid-electrolyte interfaces for $CuGaSe_2$ (left) and CdS/$CuGaSe_2$ (right) electrodes. Reprinted with permission from ref. [13b]. ©2013 American Chemical Society.

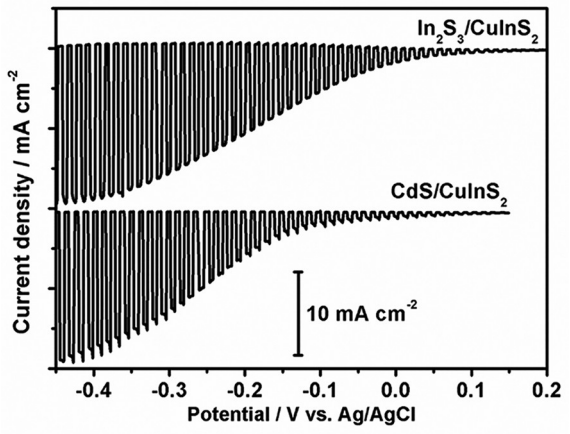

Figure 8. Current density-potential curves of CdS/$CuInS_2$ and In_2S_3/$CuInS_2$ electrodes obtained from an aqueous 0.2 M $Eu(NO_3)_3$ solution (pH 4) under chopped illumination of simulated sunlight (AM1.5). Adapted with permission from ref. [14e]. ©2015 American Chemical Society.

The other characteristic achieved over the Pt-In_2S_3/$CuInS_2$ electrode compared to that of the Pt-CdS/$CuInS_2$ electrode is the relatively positive onset potential achieved on the electrode. In order to examine these differences, current-potential curves of the In_2S_3/$CuInS_2$ electrode and the CdS/$CuInS_2$ electrode (without loadings of Pt deposits) in an 0.2 M $Eu(NO_3)_3$ solution (pH 4) were examined. Typical results are shown in Figure 8.[14e] Although both In_2S_3/$CuInS_2$ and CdS/$CuInS_2$ electrodes gave large photocurrent densities of more than 10 mA cm^{-2}, appreciable differences in photocurrent onsets were observed between current-potential curves of these electrodes: the onset potential of photocurrents obtained over the In_2S_3/$CuInS_2$ electrode (ca. 0.17 V vs Ag/AgCl) was more positive than that obtained over the CdS/$CuInS_2$ electrode (ca. 0.10 V vs Ag/AgCl), similar to those observed in the above PEC water reduction. As has been reported in the literature discussing photovoltaics based on the CdS-$CuInS_2$ heterojunction, the CdS-$CuInS_2$ interface is considered to be a "cliff-type" conduction band alignment: the CBM of CdS is deeper than that of $CuInS_2$ (i.e., ΔCBM CdS $-$ CuInS < 0). In such a band alignment, it is known that recombination at the CdS-$CuInS_2$ interface is dominant,[31] i.e., the maximum photovoltage retrieved from the CdS/$CuInS_2$ junction should be affected by such an interface recombination. Our study on evaluation of the energy diagram of the CdS/$CuInS_2$ junction using photoabsorptiion spectroscopy and XP spectroscopy also indicated an unfavorable cliff-type negative onset ($-$0.47 eV of ΔCBM), as shown in Figure 9.[14e] When the same analysis was performed for the In_2S_3/$CuInS_2$ heterojunction, it was found to have a favorable "notch-type" positive onset (0.27 eV of ΔCBM). Thus, positive shifts of onset potentials induced by using the In_2S_3/$CuInS_2$ junction should be attributed to induction of favorable modulation at the heterointerface. In the case for the use of ZnS as an alternative n-type layer,[14a] functions similar to those of In_2S_3 layer can be estimated because of its relatively negative CBM compared to that of CdS and high transparency derived from large E_g (ca. 3.7 eV), though detailed analyses regarding the ZnS/$CuInS_2$ heterojunction were not performed.

6. High Functionality of $CuGaSe_2$ Compound Semiconductor Thin Films by Controlling Their Surface Compositions

Since the E_g value of the $CuGaSe_2$ compound (1.68 eV) is larger than that of the Cu(In,Ga)Se_2 mixed crystal (Ga/(Ga + In) ratio of 0.3) used in solar cells (ca. 1.3 eV), it is expected that a thin film of $CuGaSe_2$ can be applied as a absorber in the top cell of tandem and multi-junction solar cells.[18c,32] On the other hand, attempts to use $CuGaSe_2$ as a photocathode for PEC water reduction into H_2 have been fewer than those for solar cell applications. Indeed, examples for achievements of significant

© 2024 The Authors. ChemElectroChem published by Wiley-VCH GmbH

21960216, 2024, 21, Downloaded from https://chemistry-europe.onlinelibrary.wiley.com/doi/10.1002/celc.202400365 by Chandigarh University, Wiley Online Library on [30/09/2026]. See the Terms and Conditions (https://onlinelibrary.wiley.com/terms-and-conditions) on Wiley Online Library for rules of use; OA articles are governed by the applicable Creative Commons License

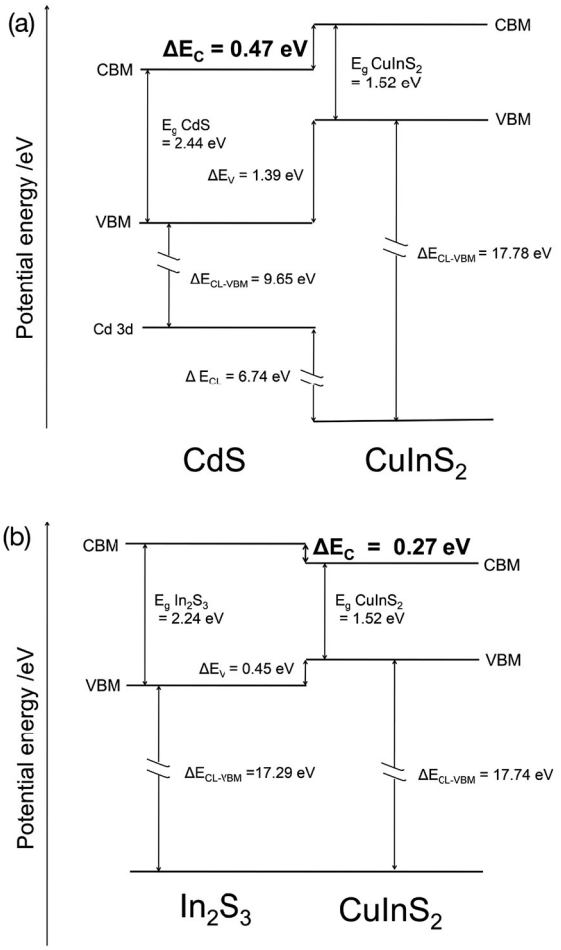

Figure 9. Energy diagrams of (a) $CdS/CuInS_2$ and (b) $In_2S_3/CuInS_2$ heterojunctions estimated from photoabsorption and XP spectroscopy results. Adapted with permission from ref. [14e]. ©2015 American Chemical Society.

PEC H_2 generation have been limited; HC-STHs obtained were below 1 %,[13b,15a] the value of which is much lower than the best value obtained over a photocathode based on a $Cu(In,Ga)Se_2$ mixed crystal (12.5 %).[13h] Thus, there is a room for further improvement of properties for PEC water reduction over the $CuGaSe_2$-based electrode.

In recent studies on the functionalization of $CuGaSe_2$-based solar cells, it has been shown that the open circuit voltage (V_{OC}) and short circuit current density (J_{SC}) can be improved by intentional deposition of a Cu-deficient layer (CDL) consisting of $CuGa_3Se_5$ and several phases with different compositions at the CdS-$CuGaSe_2$ heterointerface.[32e] We therefore aimed at similar enhancements in PEC water reduction into H_2, i.e., achievements of a shift of the photocathodic current onset potential to the positive side as well as an increase in the saturation photocurrent by applying interface modification with a CDL. For these purposes, $CuGaSe_2$ thin films coated with CDLs of different thicknesses were prepared on Mo/glass substrates by vacuum co-evaporation using a molecular beam deposition (MBD) system. Knudsen cells loaded with elemental sources of Cu, Ga, and Se were placed in the vacuum chamber of the MBD system. A $CuGaSe_2$ thin film without a CDL (w/o CDL) and $CuGaSe_2$ thin films with a CDL of less than 50 nm in thickness (CDL_<50), CDL of 50 nm in thickness (CDL_50) and CDL of 200 nm in thickness (CDL_200) were prepared by controlling the deposition duration and temperature for each elemental source. A 60-nm-thick CdS layer was deposited on each film by the CBD method. For electrodes including CDL_50 and CDL_200, deposition of a thick (90 nm) CdS layer was also applied; thus-obtained electrodes were labeled (90)CDL_50 and (90)CDL_200, respectively. Loading of Pt catalysts on all of the films was performed by the photodeposition method used in the above-described $CuInS_2$-based system. Figure 10 shows typical current-voltage curves of thus-obtained photocathodes in an electrolyte solution (0.1 M $KH_2PO_4/K_2HPO_4/K_2SO_4$ solution, pH 6.8) under simulated sunlight (AM 1.5 G) irradiation.[15a] Significant photocathodic currents for water reduction into H_2 were obtained for all of the photoelectrodes. The sum of $e^-/2$ at 0 V (vs RHE) was almost consistent with the amount of evolved H_2, indicating unity of η_F (i.e., no appreciable side reaction occurred during the PEC reduction.). Table 2 shows the HC-STH and photocurrent onset potentials for each photoelectrode estimated from the current-potential curves obtained. Compared to the results for the w/o CDL-based electrode, it is clear that both properties are significantly improved in electrodes containing a CDL. Effects of different CdS layer thicknesses on CDL_50 and CDL_200 were also noticeable: electrodes composed of a 90-nm thick CdS layer showed further enhancements of both properties compared to those obtained over the electrodes composed of a 60-nm thick CdS layer. A maximum HC-STH value of 6.6 % was achieved for (90)CDL_50 and the most positive photocathode current onset potential (0.93 V vs RHE) was obtained over (90)CDL_200.

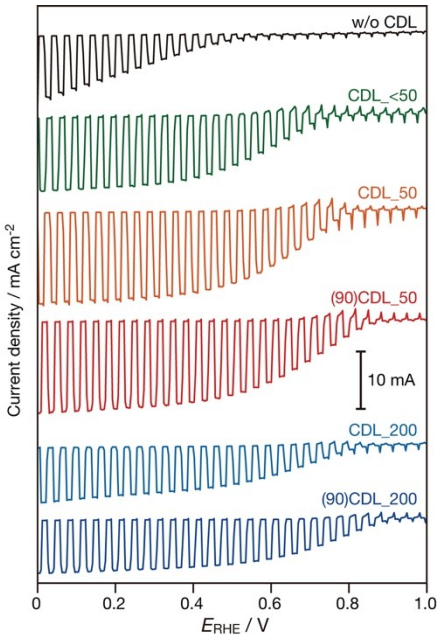

Figure 10. LSV plots of various photocathodes derived from a CuGaSe2 film and that covered with a CDL with different thicknesses measured under chopped illumination from simulated solar irradiation (AM 1.5 G). Adapted with permission from ref. [15b]. ©2021 AIP Publishing.

© 2024 The Authors. ChemElectroChem published by Wiley-VCH GmbH

21960216, 2024, 21, Downloaded from https://chemistry-europe.onlinelibrary.wiley.com/doi/10.1002/celc.202400365 by Chandigarh University, Wiley Online Library on [30/09/2026]. See the Terms and Conditions (https://onlinelibrary.wiley.com/terms-and-conditions) on Wiley Online Library for rules of use; OA articles are governed by the applicable Creative Commons License

Table 2. HC-STHs and photocurrent onset potentials of various $CuGaSe_2$-based photoelectrodes.

Electrode	HC-STH (%)	Onset E_{RHE}/V
w/o CDL[a]	1.3	0.63
CDL_<50[a]	4.4	0.77
CDL_50[a]	6.3	0.83
CDL_200[a]	6.6	0.86
90-CDL_50[a]	3.3	0.87
90-CDL200[a]	4.2	0.93
120-CDL50[a]	7.2	0.91

[a] Acronyms are noted in the main text.

In order to examine differences in PEC properties between the electrodes, the relative positions of the band edge energies of CdS, CDL and $CuGaSe_2$ were compared. Figure 11 shows estimated energy positions of the CBM and VBM of these compounds with respect to E_{RHE} calculated from those values given with respect to vacuum level.[32e] For CDL, the n-type $CuGa_3Se_5$ compound is assumed for convenience because it would be the most probable component in view of a phase diagram of the pseudo-binary Cu_2Se-Ga_2Se_3 system. The presence of the $CuGa_3Se_5$ phase as the main component in the CDL is also suggested by the observation of photoluminescence (PL) emission at the wavelength of around 670 nm (1.85 eV), corresponding to E_g of $CuGa_3Se_5$, on a CDL-covered $CuGaSe_2$ thin film. Since the $CuGa_3Se_5$ compound is known to be n-type, insertion of the layer induced a shift of the p-n junction from the CdS-$CuGaSe_2$ interface to the CDL-$CuGaSe_2$ interface, whereby the CDL blocks the diffusion of holes generated by $CuGaSe_2$ to the CdS side, while the CDL increases the spatial distance for electrons injected into the CdS side. These effects are thought to suppress carrier recombination at the CdS-$CuGaSe_2$ junction interface and improve the above-mentioned properties. The lower HC-STH of (90)CDL_200 than that of (90)CDL_50 is likely to be due to the absorption of incident light by the thick CDL layer. Based on these trends, a photoelectrode with a CDL thickness as thin as that of (90)CDL_50 and a thicker CdS layer (120 nm) was prepared (labeled (120)CDL_50); the electrode loaded with Pt catalysts achieved significant enhancement of PEC properties with HC-STH above 7%.[15b] This HC-STH efficiency is the highest among the values reported for $CuGaSe_2$-based photocathodes to date. Although HC-STH efficiencies of more than 10% have been shown for narrow-E_g Cu(In,Ga)Se_2-based photocathodes (see above), the maximum onset potential of the Cu(In,Ga)Se_2-based photocathode is relatively low (E_{RHE} <0.75 V). The $CuGaSe_2$-based photocathode exhibited an onset potential higher than 0.9 V (vs RHE) in this study.

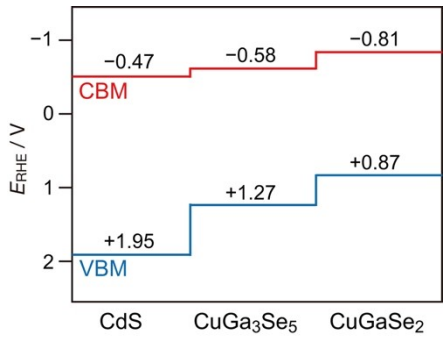

Figure 11. Relative CBM and VBM energies of $CuGaSe_2$, $CuGa_3Se_5$ (CDL), and CdS compounds.

7. Durability Issue

When a photocathode is used for PEC water reduction in a tandem system in combination with an oxygen-evolving photocathode, half of the thermodynamically required voltage (1.23 V) for overall water splitting must be covered by the photocathode side. For a three-electrode system evaluating half of the H_2 evolution reaction, this corresponds to a requirement for inducing efficient H_2 evolution at an operating potential of ca. 0.6 V (vs RHE). Judging from the current-potential curves of CDL-covered $CuGaSe_2$-based photocathodes shown in Figure 11, these photoelectrodes are capable. However, when the reaction was performed at potentials near 0.6 V (vs RHE), a significant decrease in H_2 production along with a gradual decline of photocurrent flow was observed for these photocathodes, as shown in Figure 12.[15b] A similar decrease in PEC properties for water reduction has also been observed for photoelectrode based on Pt-CdS-modified $CuInS_2$[14c,e] and other Cu-based p-type chalcogenide compounds of Cu_2ZnSnS_4.[33] Analyses of surface properties of a Cu_2ZnSnS_4-based photoelectrode (i.e., Pt-CdS/Cu_2ZnSnS_4) layer by SEM and XP spectroscopy indicated occurrence of significant degradation of the surface-covered CdS layer.[33] In order to suppress this degradation, therefore, attempts to coat the CdS surface with another compound layer as a "protective layer" have been made. The

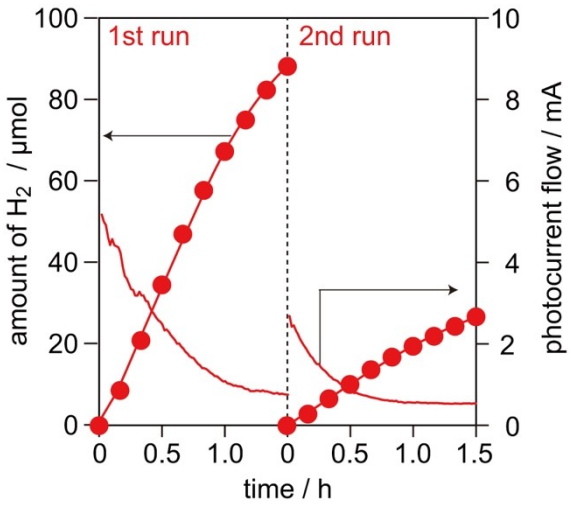

Figure 12. Time course curve of H_2 evolution and photocurrent profile over the photocathode based on the (90)CDL_50 thin film at 0.5 V vs RHE. Adapted with permission from ref. [15b]. ©2021 AIP Publishing.

© 2024 The Authors. ChemElectroChem published by Wiley-VCH GmbH

21960216, 2024, 21, Downloaded from https://chemistry-europe.onlinelibrary.wiley.com/doi/10.1002/celc.202400365 by Chandigarh University, Wiley Online Library on [30/09/2026]. See the Terms and Conditions (https://onlinelibrary.wiley.com/terms-and-conditions) on Wiley Online Library for rules of use; OA articles are governed by the applicable Creative Commons License

21960216, 2024, 21, Downloaded from https://chemistry-europe.onlinelibrary.wiley.com/doi/10.1002/celc.202400365 by Chandigarh University, Wiley Online Library on [30/09/2026]. See the Terms and Conditions (https://onlinelibrary.wiley.com/terms-and-conditions) on Wiley Online Library for rules of use; OA articles are governed by the applicable Creative Commons License

most common compound used for the corrosion protection is TiO_2 due to its high stability in an electrolyte, suitable band structure, and availability. Indeed, significant improvements of durability induced by the protection of TiO_2 have been proved by several groups.[34] For the Cu_2ZnSnS_4-based system, moreover, coverage of the surface of the CdS layer with In_2S_3[33] or HfO_2[35] was also effective for improving stability of photocurrents. Since the introduction of a protective layer is applicable to all kinds of CdS-covered photocathodes, this coating process should also be suitable for several chalcopylyte-based photocathodes including $CuInS_2$ and $CuGaSe_2$.

8. Summary and Outlook

In this review, historical backgrounds, operation principles, analytical methods, and findings from the early days to the current state-of-the-art research of PEC water splitting for H_2 production under sunlight irradiation were introduced with focus on photocathodes composed of Cu-based chalcopyrite compound ($CuInS_2$ and $CuGaSe_2$) thin films that were developed by our group. Since the hypothetical efficiency (HC-STH) in the system introduced in this review is still below 10%, a significant breakthrough for further improvement is necessary for its practical use. Although not presented in this review, we have recently found that rubidium (Rb) doping improved the HC-STH by up to 8% over a $CuGaSe_2$-based photocathode.[15b] However, the achievement still does not reach the level necessary for practical use. In addition to the efficiency issue, moreover, suppression of deterioration is still a critical issue that needs to be further improved. Instead of the use of a protection layer introduced herein, a simple idea for improving stability is to replace the unstable CdS layer with another n-type component. In this regard, the In_2S_3 layer used for the $CuInS_2$-based photocathode system seemed to be effective but was not sufficient: a gradual decrease in the photocurrent was observed even in a highly cathodic biased condition (0 V vs RHE).[14b] Regarding the $CuGaSe_2$ thin film, recent studies on solar cells have shown that application of a ZnSnO layer as an alternative n-type layer provides better performance than that of the conventional CdS layer,[36] though there has been no report on the achievement of PEC performance comparable to that with the use of a CdS layer. In addition, replacements of rare elements used such as Pt as catalysts for H_2 production are also required. Several materials, including metal chalcogenides[37] and alloys[38] have been studied for this purpose. Suitable designs of PEC cells of a tandem configuration for scaling up at a low cost also remains a charenge.[12] We hope that new players will emerge from among the readers in order to provide a more practical direction.

Acknowledgements

The results cited in this article are those of a joint research project with Prof. Emer. Michio Matsumura (Osaka University), Dr. Takashi Harada, Prof. Kazunari Domen (Shinshu University & The University of Tokyo), Assoc. Prof. Yoshitaro Nose (Kyoto University), Prof. Jiang Feng (South China Normal University), and our students and colleagues. This work was financially supported by JSPS KAKENHI (Nos. 23K26600 and 23K26767), and Bilateral Programs (No. JPJSPB120247415). This work was also supported by the Hirao Taro Foundation of KONAN GAKUEN for Academic Research (No. 202201).

Conflict of Interests

The authors declare no conflict of interest.

Data Availability Statement

The data that support the findings of this study are available from the corresponding author upon reasonable request.

Keywords: Photoelectrochemical water reduction · Photocathode · Chalcopyrite thin films

[1] Energy Institute. *The Energy Institute Statistical Review of World Energy 2023*. **2023**.
[2] International Energy Agency. *IEA Key world energy statistics 2021*, **2021**.
[3] The National Aeronautics and Space Administration. *The Balance of Power in the Earth*, **2005**.
[4] a) S. Y. Reece, J. A. Hamel, K. Sung, T. D. Jarvi, A. J. Esswein, J. J. H. Pijpers, D. G. Nocera, *Scinece* **2011**, *29*, 645; b) A. Nakamura, Y. Ota, K. Koike, Y. Hidaka, K. Nishioka, M. Sugiyama, K. Fujii, *Appl. Phys. Express* **2015**, *8*, 107101; c) Z. N. Zahran, Y. Miseki, E. A. Mohamed, Y. Tsubonouchi, K. Makita, T. Sugaya, K. Sayama, M. Yagi, *ACS Appl. Energy Mater.* **2022**, *5*, 8241
[5] C. A. Rodriguez, M. A. Modestino, D. Psaltis, C. Moser, *Energy Environ. Sci.* **2014**, *7*, 3828.
[6] a) F. T. Wagner, G. A. Somorjai, *J. Am. Chem. Soc.* **1980**, *102*, 5494; b) K. Domen, S. Naito, T. Onishi, K. Tamaru, *Chem. Phys. Lett.* **1982**, *92*, 433; c) K. Domen, A. Kudo, T. Onishi, *J. Catal.* **1986**, *102*, 92; d) K. Domen, A. Kudo, T. Onishi, N. Kosugi, H. Kuroda, *J. Phys. Chem.* **1986**, *90*, 292
[7] a) A. Kudo, A. Tanaka, K. Domen, K. Maruya, K. Aika, T. Onishi, *J. Catal.* **1988**, *111*, 67; b) Y. Inoue, T. Niiyama, Y. Asai, K. Sato, *J. Chem. Soc. Chem. Commun.* **1992**, 579; c) S. Ikeda, M. Hara, J. N. Kondo, K. Domen, H. Takahashi, T. Okubo, M. Kakihana, *Chem. Mater.* **1998**, *10*, 72; d) H. Kato, A. Kudo, *Chem. Phys. Lett.* **1998**, *295*, 487; e) S. Ikeda, T. Itani, K. Nango, M. Matsumura, *Catal. Lett.* **2004**, *98*, 229; f) J. Sato, N. Saito, Y. Yamada, K. Maeda, T. Takata, J. N. Kondo, M. Hara, H. Kobayashi, K. Domen, Y. Inoue, *J. Am. Chem. Soc.* **2005**, *127*, 4150; g) S. Ikeda, M. Fubuki, Y. K. Takahara, M. Matsumura, *Appl. Catal., A* **2006**, *300*, 186; h) K. Maeda, K. Teramura, D. Lu, T. Takata, N. Saito, Y. Inoue, K. Domen, *Nature* **2006**, *440*, 295; i) S. Ikeda, K. Hirao, S. Ishino, M. Matsumura, B. Ohtani, *Catal. Today* **2006**, *117*, 343; j) T. Takata, K. Domen, *J. Phys. Chem. C* **2009**, *113*, 19386; k) T. Takata, C. Pan, M. Nakabayashi, N. Shibata, K. Domen, *J. Am. Chem. Soc.* **2015**, *137*, 9627
[8] a) Y. Ham, T. Hisatomi, Y. Goto, Y. Moriya, Y. Sakata, A. Yamakata, J. Kubota, K. Domen, *J. Mater. Chem. A* **2016**, *4*, 3027; b) Y. Goto, T. Hisatomi, Q. Wang, T. Higashi, K. Ishikiriyama, T. Maeda, Y. Sakata, S. Okunaka, H. Tokudome, M. Katayama, S. Akiyama, H. Nishiyama, Y. Inoue, T. Takewaki, T. Setoyama, T. Minegishi, T. Takata, T. Yamada, K. Domen, *Joule* **2018**, *2*, 509; c) T. H. Chiang, H. Lyu, T. Hisatomi, Y. Goto, T. Takata, M. Katayama, T. Minegishi, K. Domen, *ACS Catal.* **2018**, *8*, 2782; d) H. Lyu, T. Hisatomi, Y. Goto, M. Yoshida, T. Higashi, M. Katayama, T. Takata, T. Minegishi, H. Nishiyama, T. Yamada, Y. Sakata, K. Asakura, K. Domen, *Chem. Sci.* **2019**, *10*, 3196; e) T. Takata, J. Jiang, Y. Sakata, M. Nakabayashi, N. Shibata, V. Nandal, K. Seki, T. Hisatomi, K. Domen, *Nature* **2020**, *581*, 411; f) S. Ikeda, R. Okamoto, A. Kimura, Y. Nakayasu, A. Yamakata, R. Tomizawa, T. Masuda, K. Nakatani, *Sustain. Energy Fuels* **2024**, *8*, 202

© 2024 The Authors. ChemElectroChem published by Wiley-VCH GmbH

21960216, 2024, 21, Downloaded from https://chemistry-europe.onlinelibrary.wiley.com/doi/10.1002/celc.202400365 by Chandigarh University, Wiley Online Library on [30/09/2026]. See the Terms and Conditions (https://onlinelibrary.wiley.com/terms-and-conditions) on Wiley Online Library for rules of use; OA articles are governed by the applicable Creative Commons License

[9] a) R. Abe, K. Sayama, H. Sugihara, *J. Phys. Chem. B* **2005**, *109*, 16052; b) R. Abe, *J. Photochem. Photobiol. C: Photochem. Rev.* **2010**, *11*, 179; c) A. Iwase, Y. H. Ng, Y. Ishiguro, A. Kudo, R. Amal, *J. Am. Chem. Soc.* **2011**, *133*, 11054; d) Y. Wang, H. Suzuki, J. Xie, O. Tomita, D. J. Martin, M. Higashi, D. Kong, R. Abe, *J. Tang, Chem. Rev.* **2018**, *118*, 5201; e) Q. Wang, T. Hisatomi, Q. Jia, H. Tokudome, M. Zhong, C. Wang, Z. Pan, T. Takata, M. Nakabayashi, N. Shibata, Y. Li, I. D. Sharp, A. Kudo, T. Yamada, K. Domen, *Nat. Mater.* **2016**, *15*, 611; f) Q. Wang, T. Hisatomi, Y. Suzuki, Z. Pan, J. Seo, M. Katayama, T. Minegishi, H. Nishiyama, T. Takata, K. Seki, A. Kudo, T. Yamada, K. Domen, *J. Am. Chem. Soc.* **2017**, *139*, 1675

[10] N. W. Ockwig, T. M. Nenoff, *Chem. Rev.* **2007**, *107*, 4078.

[11] a) M. Grätzel, *Nature* **2001**, *414*, 338; b) M. G. Walter, E. L. Warren, J. R. McKone, S. W. Boettcher, Q. Mi, E. A. Santori, N. S. Lewis, *Chem. Rev.* **2010**, *110*, 6446; c) T. Hisatomi, J. Kubota, K. Domen, *Chem. Soc. Rev.* **2014**, *43*, 7520; d) Y. Chen, X. Feng, M. Liu, J. Su, S. Shen, *Nanophotonics* **2016**, *5*, 524; e) C. Ding, J. Shi, Z. Wang, C. Li, *ACS Catal.* **2017**, *7*, 675; f) T. Yao, H. Han, J. Q. Chen, C. Li, *Adv. Energy Mater.* **2018**, *8*, 1800210; g) K. Zhang, M. Ma, P. Li, D. H. Wang, J. H. Park, *Adv. Energy Mater.* **2016**, *6*, 1600602

[12] A. Vilanova, P. Dias, T. Lopes, A. Mendes, *Chem. Soc. Rev.* **2024**, *53*, 2388.

[13] a) D. Yokoyama, T. Minegishi, K. Maeda, M. Katayama, J. Kubota, A. Yamada, M. Konagai, K. Domen, *Electrochem. Commun.* **2010**, *12*, 851; b) M. Moriya, T. Minegishi, H. Kumagai, M. Katayama, J. Kubota, K. Domen, *J. Am. Chem. Soc.* **2013**, *135*, 3733; c) H. Kumagai, T. Minegishi, Y. Moriya, J. Kubota, K. Domen, *J. Phys. Chem. C* **2014**, *118*, 16386; d) M. G. Mali, H. Yoon, B. N. Joshi, H. Park, S. S. Al-Deyab, D. C. Lim, S. Ahh, C. Nervi, *ACS Appl. Mater. Interfaces* **2015**, *7*, 21619; e) H. Kaneko, T. Minegishi, M. Nakabayashi, N. Shibata, Y. Kuang, T. Yamada, K. Domen, *Adv. Funct. Mater.* **2016**, *26*, 4570; f) N. Guijarro, M. S. Prévot, X. Yu, X. A. Jeanbourquin, P. Bornoz, W. Bourée, M. Johnson, F. L. Formal, K. Sivula, *Adv. Energy Mater.* **2016**, *6*, 1501949; g) A. D. DeAngelis, K. Horsley, N. Gaillard, *J. Phys. Chem. C* **2018**, *122*, 14304; h) H. Kobayashi, N. Sato, M. Orita, Y. Kuang, H. Kaneko, T. Minegishi, T. Yamada, K. Domen, *Energy Environ. Sci.* **2018**, *11*, 3003; i) M. Chen, Y. Liu, C. Li, A. Li, X. Chang, W. Liu, Y. Sun, T. Wang, J. Gong, *Energy Environ. Sci.* **2018**, *11*, 2025; j) B. Kim, G. S. Park, Y. J. Hwang, D. H. Won, W. Kim, D. K. Lee, B. K. Min, *ACS Energy Lett.* **2019**, *4*, 2937

[14] a) S. Ikeda, T. Nakamura, S. M. Lee, T. Yagi, T. Harada, T. Minegishi, M. Matsumura, *ChemSusChem* **2011**, *4*, 262–268; b) Gunawan, W. Septina, S. Ikeda, T. Harada, T. Minegishi, K. Domen, M. Matsumura, *Chem. Commun.* **2014**, *50*, 8941; c) J. Zhao, T. Minegishi, L. Zhang, M. Zhong, Gunawan, M. Nakabayashi, G. Ma, T. Hisatomi, M. Katayama, S. Ikeda, N. Shibata, T. Yamada, K. Domen, *Angew. Chem. Int. Ed.* **2014**, *53*, 11808; d) W. Septina, Gunawan, S. Ikeda, T. Harada, T. Higashi, R. Abe, M. Matsumura, *J. Phys. Chem. C* **2015**, *119*, 8576; e) Gunawan, Septina, T. Harada, Y. Nose, S. Ikeda, *ACS Appl. Mater. Interfaces* **2015**, *7*, 16086; f) W. Septina, M. Sugimoto, D. Chao, Q. Shen, S. Nakatsuka, Y. Nose, T. Harada, S. Ikeda, *Phys. Chem. Chem. Phys.* **2017**, *19*, 12502

[15] a) S. Ikeda, S. W. Fujita, R. Okamoto, Y. Nose, R. Katsube, K. Yoshino, T. Harada, *RSC Adv.* **2020**, *10*, 40310; b) S. Ikeda, R. Okamoto, S. Ishizuka, *Appl. Phys. Lett.* **2021**, *119*, 083902; c) S. Ishizuka, R. Okamoto, S. Ikeda, *Adv. Mater. Interfaces* **2022**, *9*, 2201266

[16] a) R. Saniz, J. Bekaert, B. Partoens, D. Lamoen, *Phys. Chem. Chem. Phys.* **2017**, *19*, 14770–14780; b) T. Wada, *JSAP Rev.* **2022**, *2022*, 220204

[17] a) Y. Kumagai, M. Choi, Y. Nose, F. Oba, *Phys. Rev. B* **2014**, *90*, 125202; b) S. Nakatsuka, Y. Nose, *J. Phys. Chem. C* **2017**, *121*, 1040

[18] a) M. I. Alonso, K. Wakita, J. Pascual, M. Garriga, N. Yamamoto, *Phys. Rev. B* **2001**, *63*, 075203; b) S. Lany, A. Zunger, *Phys. Rev. Lett.* **2008**, *100*, 016401; c) S. Ishizuka, *Phys. Status Solidi A* **2019**, *216*, 1800873; d) T. Maeda, R. Nakanishi, M. Yanagita, T. Wada, *Jpn. J. Appl. Phys.* **2020**, *59*, SGGF12; e) R. Yoneda, K. Beppu, T. Maeda, and T. Wada, *Jpn. J. Appl. Phys.* **2022**, *61*, SC180.

[19] a) S. Niki, M. Contreras, I. Repins, M. Powalla, K. Kushiya, S. Ishizuka, K. Matsubara, *Prog. Photovolt.: Res. Appl.* **2010**, *18*, 453; b) J. Nishinaga, Y. Kamikawa, T. Sugaya, S. Ishizuka, *Sol. Energy Mater. Sol. Cells* **2024**, *269*, 112791.

[20] M. Nakamura, K. Yamaguchi, Y. Kimoto, Y. Yasaki, T. Kato, H. Sugimoto, *IEEE J. Photovolt.* **2019**, *9*, 1863.

[21] M. A. Green, E. D. Dunlop, J. Hohl-Ebinger, M. Yoshita, N. Kopidakis, X. Hao, *Prog. Photovolt.* **2021**, *29*, 657.

[22] a) S. B. Zhang, S.-H. Wei, A. Zunger, H. Katayama-Yoshida, *Phys. Rev. B* **1998**, *57*, 9642; b) S.-H. Wei, S. B. Zhang, *J. Phys. Chem. Solids* **2005**, *66*, 1994.

[23] a) C. Persson, A. Zunger, *Appl. Phys. Lett.* **2005**, *87*, 211904; b) S. Siebentritt, S. Sadewasser, M. Wimmer, C. Leendertz, T. Eisenbarth, M. C. Lux-Steiner, *Phys. Rev. Lett.* **2006**, *97*, 146601; c) Y. Yan, C.-S. Jiang, R. Noufi, S.-H. Wei, H. R. Moutinho, M. M. Al-Jassim, *Phys. Rev. Lett.* **2007**, *99*, 235504; d) J. Kavalakkatt, D. Abou-Ras, J. Haarstrich, C. Ronning, M. Nichterwitz, R. Caballero, T. Rissom, T. Unold, R. Scheer, H.-W. Schock, *J. Appl. Phys.* **2014**, *115*, 014504; e) M. Raghuwanshi, B. Thöner, P. Soni, M. Wuttig, R. Wuerz, O. Cojocaru-Miredin, *ACS Appl. Mater. Interfaces* **2018**, *10*, 14759.

[24] K. Sivula, *J. Phys. Chem. Lett.* **2013**, *4*, 1624.

[25] M. S. Prévot, K. Sivula, *J. Phys. Chem. C* **2013**, *177*, 17879.

[26] A. Kudo, Y. Miseki, *Chem. Soc. Rev.* **2009**, *38*, 253.

[27] a) D. Lincot, H. Gomez Meier, J. Kessler, J. Vedel, B. Dimmler, H. W. Schock, *Sol. Energy Mater.* **1990**, *20*, 67; b) J. J. Scragg, P. J. Dale, L. M. Peter, G. Zoppi, I. Forbes, *Phys. Status Solidi B* **2008**, *245*, 1772; c) S. M. Lee, S. Ikeda, T. Yagi, T. Harada, A. Ennaoui, M. Matsumura, *Phys. Chem. Chem. Phys.* **2011**, *13*, 6662

[28] a) S. M. Lee, S. Ikeda, T. Harada, M. Matsumura, *J. Non-Cryst. Solids.* **2012**, *358*, 2424; b) S. M. Lee, S. Ikeda, Y. Otsuka, T. Harada, M. Matsumura, *Electrochim. Acta* **2012**, *79*, 189

[29] a) J. Klaer, J. Bruns, R. Henninger, K. Siemer, R. Klenk, K. Ellmer, D. Bräunig, *Semicond. Sci. Technol.* **1998**, *13*, 1456; b) A. Ennaoui, M. Bär, J. Klaus, T. Kropp, R. Saez-Araoz, M. C. Lux-Steiner, *Prog. Photovolt. Res. Appl.* **2006**, *14*, 499

[30] a) M. A. Butler, *J. Appl. Phys.* **1977**, *48*, 1914; b) T. Torimoto, S. Takabayashi, H. Mori, S. Kuwabata, *J. Electroanal. Chem.* **2002**, *522*, 33

[31] a) T. Minemoto, T. Matsui, H. Takakura, Y. Hamakawa, T. Negami, Y. Hashimoto, T. Uenoyama, M. Kitagawa, *Sol. Energy Mater. Sol Cells* **2001**, *67*, 83; b) C. Ding, Y. Zhang, F. Liu, Y. Kitabatake, S. Hayase, T. Toyoda, K. Yoshino, T. Minemoto, K. Katayama, Q. Shen, *Nano Energy* **2018**, *53*, 17

[32] a) M. Saad, H. Riazi, E. Bucher, M. C. Lux-Steiner, *Appl. Phys. A* **1996**, *62*, 181; b) D. L. Young, J. Keane, A. Duda, J. A. M. AbuShama, C. L. Perkins, M. Romero, R. Noufi, *Prog. Photovolt. Res. Appl.* **2003**, *11*, 535; c) S. Ishizuka, A. Yamada, P. J. Fons, H. Shibata, S. Niki, *Appl. Phys. Lett.* **2013**, *103*, 143903; d) F. Larsson, N. S. Nilsson, J. Keller, C. Frisk, V. Kosyak, M. Edoff, T. Törndahl, *Prog. Photovolt. Res. Appl.* **2017**, *25*, 755; e) S. Ishizuka, *Appl. Phys. Lett.* **2021**, *118*, 133901

[33] F. Jiang, T. Gunawan, *J. Am. Chem. Soc.* **2015**, *137*, 13691.

[34] a) B. Koo, S.-W. Nam, R. Haight, S. Kim, S. Oh, M. Cho, J. Oh, J. Y. Lee, B. T. Ahn, B. Shin, *ACS Appl. Mater. Interfaces* **2017**, *9*, 5279; b) Y. Kageshima, T. Fujita, F. Takagi, T. Minegishi, K. Teshima, K. Domen, Y. Amao, H. Nishikiori, *ChemElectroChem* **2019**, *6*, 4859; c) M. Chen, Y. Liu, C. Li, A. Li, X. Chang, W. Liu, Y. Sun, T. Wang, J. Gong, *Energy Environ. Sci.* **2018**, *11*, 2025

[35] a) D. Huang, K. Wang, L. Yu, T. H. Nguyen, S. Ikeda, F. Jiang, *ACS Energy Lett.* **2018**, *3*, 1875; b) D. Huang, K. Wang, L. Li, K. Feng, N. An, S. Ikeda, Y. Kuang, Y. Ng, F. Jiang, *Energy Environ. Sci.* **2021**, *14*, 1480

[36] F. Larsson, N. S. Nilsson, J. Keller, C. Frisk, V. Kosyak, M. Edoff, T. Törndahl, *Prog. Photovolt.* **2017**, *25*, 755.

[37] a) M. Wang, Y.-S. Chang, C.-W. Tsao, M.-J. Fang, Y.-J. Hsu, K.-L. Choy, *Chem. Commun.* **2019**, *55*, 2465; b) B. Kim, G. S. Park, Y. J. Hwang, D. H. Won, W. Kim, D. K. Lee, B. K. Min, *ACS Energy Lett.* **2019**, *4*, 2937

[38] M. Baek, M. Zafar, S. Kim, D. H. Kim, C. W. Jeon, J. Lee, K. Yong, *ChemSusChem.* **2018**, *11*, 3679.

Manuscript received: May 13, 2024
Revised manuscript received: August 29, 2024
Version of record online: October 21, 2024

© 2024 The Authors. ChemElectroChem published by Wiley-VCH GmbH